Journal of Marine Research, 63, 315–333, 2005

Speculations on a schematic theory of the Younger Dryas

by Carl Wunsch[1]

ABSTRACT

The possible implications of a change in deep ocean mixing generated by the abrupt coverage of continental shelves during deglaciation is explored schematically. A simple Cartesian continental shelf/deep ocean tidal model is used to mimic the behavior of tidal dissipation at a variety of frequencies relative to a basin-near-resonance. The actual estimated sea level curve is then used to calculate a representative deep water tidal dissipation through time, which is then translated by means of a one-dimensional loop flow to explore the implications of a change in deep ocean mixing. It is possible to pick parameters for the loop model, which is analogous to the Stommel two-state box model, such that interesting transitions occur when diffusion alone is changed, including oscillatory responses. To the extent that the box model is believed to mimic the ocean circulation, it can produce shifts analogous to the re-glaciation and subsequent de-glaciation characterizing the Younger Dryas interval. That changing topography and winds would likely also have a profound influence on mixing by mesoscale disturbances is noted but not pursued.

1. Introduction

The so-called Younger Dryas (YD) is an interval about 12,000 years before present, when the ongoing de-glaciation following the last ice age appears to have abruptly ceased, and an interval of re-glaciation lasting about 1000 years ensued. De-glaciation then re-commenced, ending in the climate of today (e.g., Bradley, 1999). Evidence for this chain of events is clearest in the North Atlantic sector. Existing explanations for the YD have focussed on the role of freshwater contributions from melting ice and the supposition that a major buoyancy input to the North Atlantic Ocean would profoundly diminish the meridional mass flux. One is left to infer that the meridional oceanic heat transport and sea-surface temperatures similarly would be reduced (e.g., Bradley, 1999; Saltzman, 2002) leading to a colder climate in the vicinity of the North Atlantic basin. Nilsson *et al.* (2003) and others have proposed a different outcome for the convective response of the ocean to a freshwater pulse, but that physics is not taken up here. Note, however, that a reduced meridional transport of heat by the ocean would result in a net warming (or moistening) of

1. Department of Earth, Atmospheric and Planetary Sciences, Massachusetts Institute of Technology, Cambridge, Massachusetts, 02139, U.S.A. ***email: cwunsch@mit.edu***

the atmosphere as the total transport of heat toward the poles by the combined ocean/atmosphere system has to be maintained—whatever the regional shifts might be.

The purpose of this present note is to sketch an alternative to the hypothesis of a buoyancy-forced reduction in the oceanic heat flux, one that would act both regionally in the North Atlantic, and globally. At best, it is a mechanism, rather than a complete theory. We point at a process—whose presence can potentially have profound consequences for the ocean circulation—that cannot apparently be excluded out of hand. Actual test of its importance to climate will have to await skillful high resolution coupled atmosphere/ocean/cryosphere models.

2. A mechanism

Munk and Wunsch (1998) suggested that much of the oceanic meridional overturning circulation, and probably the associated heat flux by the ocean, were limited by the ability of the ocean to mix dense bottom waters across the stable stratification of the abyss (a subsequent review can be found in Wunsch and Ferrari, 2004). The gist of the story is that the deep ocean is stably stratified (the parameter, $N/f \gg 1$, almost everywhere, where N is the buoyancy frequency and f the Coriolis parameter; see, e.g., Gill, 1982), and that transferring abyssal water back to the surface to complete the circuit of bottom water formation requires an external energy source supporting the turbulence required to carry out the implied mixing. Their estimate was that about 2 Terrawatts ($2\ \mathrm{TW} = 2 \times 10^{15}$ W) of external mechanical energy was required, and that up to 1/2 of that energy is probably being provided by tidal mixing in the deep ocean. All numbers are very uncertain.

In the present ocean, approximately half the dissipation of tidal energy lies on the continental shelves (Munk and Wunsch, 1998) of water depth of order 100 m. During the last glacial maximum, sea level was drawn down by 120+ m (Fairbanks, 1989), an effect that would have reduced the tidal dissipation by a considerable factor. In a simple world, one could infer that under these circumstances the deep water tide would have increased, and the induced abyssal mixing by the tides would also have increased and led to a modified general circulation. As the de-glaciation took place, there would be a transitional state, in which the continental shelves would have become covered initially with a shallow fluid layer, with potentially vigorous tidal flow and dissipation, greatly reducing the available abyssal mixing. As the continental ice sheets continued to melt, the water depth over the continental shelves would have gradually increased. Depending upon the dynamical details, the increasing water depth could have modified the tidal dissipation on the shelves, with corresponding shifts in deep water, until modern values were reached. Determining how the ocean circulation would have changed in the transient and hypothetical equilibrium states as deep water mixing changes in time requires a detailed and accurate computation with a complete general circulation model.

What one can do without such a computation is to explore the possibility that a reduction, abrupt or gradual, in deep ocean mixing rates caused by the flooding of the

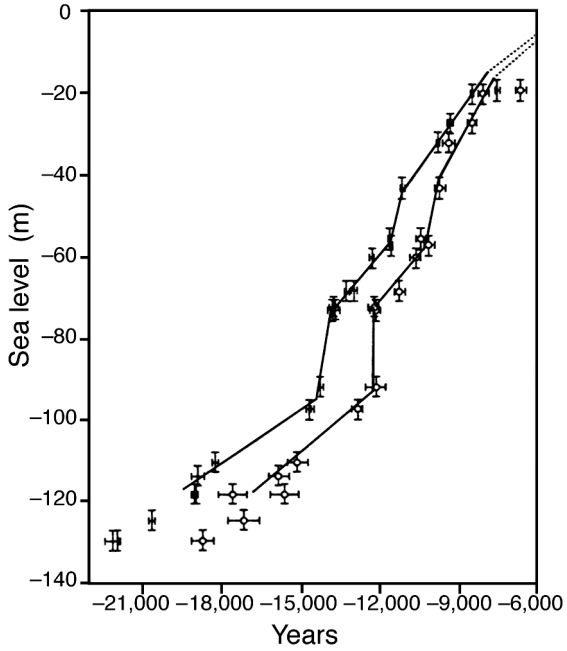

Figure 1. Redrawn from Bard *et al.* (1990), with time reversed to increase from left to right. Upper curve is estimated sea level with respect to today using Barbados terraces and U/Th dates. Lower curve is identical except that ^{14}C dates are used. U/Th dates are believed more accurate, but many other variables are specified relative to ^{14}C. A 7 meter adjustment for the greater height of the last interglacial was made by Bard *et al.* (1990).

continental shelves changed the ocean circulation such that the net heat budget and/or oceanic surface temperatures produced a major climate shift. As the system adjusted to the changed mixing, one can postulate an eventual recovery leading to a renewed deglaciation. The purpose of this note is to render this scenario somewhat plausible, but without making any claim to describing a realistic chain of events.

3. The sea level change, tidal mixing, and other energy sources

The Bard *et al.* (1990) curves (Fig. 1) appears to be the most widely accepted estimate of sea level change during the last deglacial interval. It is based upon the Barbados terrace work of Fairbanks (1989), as modified by later U/Th dates. Note the rapid rise at times just older than −12,000 y (we will use radiocarbon dates because, as in Fig. 2, they have been most commonly used to label contemporaneous events). Negative dates refer to time prior to the present. Figure 2 shows a reconstruction, with some temporal adjustment, by Lehman and Keigwin (1992) of climate proxies apparently depicting the YD and compared with the time derivative of a smoothed version of the Fairbanks (1989) curve. The two

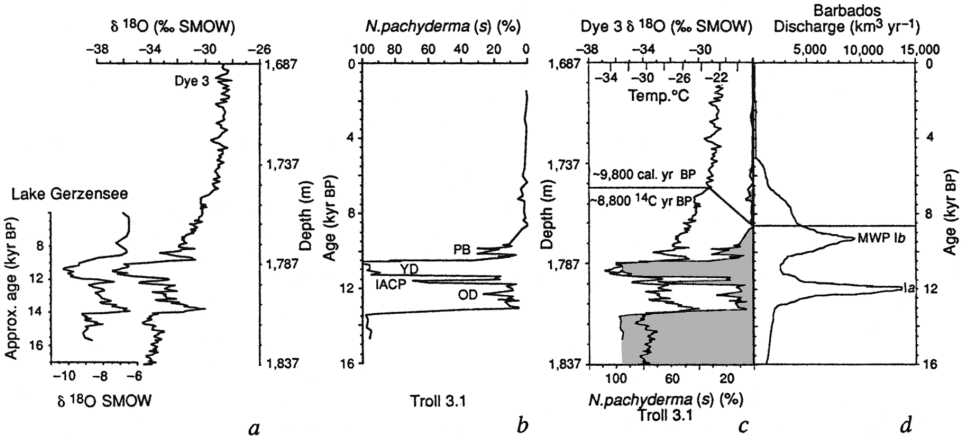

Figure 2. From Lehman and Keigwin (1992) showing (a) $\delta^{18}O$ in a Swiss lake, and from the Dye 3 core in Greenland; (b) percentage of *N. pachyderma* in an ocean core; (c) overlain ocean and ice core $\delta^{18}O$ records; and (d) the time derivative of the Barbados sea level curve. See Lehman and Keigwin (1992) for details. YD indicates the Younger Dryas interval. Some adjustments have been made to these records to increase their visual correlations in time. Note that meltwater pulse 1a at about 12,000 ^{14}C years before the present just precedes the YD in this rendering.

striking meltwater pulses (MWP) should not be taken overly seriously, as they are obtained from differentiation of the noisy and not completely understood sea level curves. Fortunately, the results obtained below do not depend upon details of the sea level curve, merely the general rise.

The present-day global hypsometric curve (cumulative area between −300 m and 0 m, from ETOP05) is shown in Figure 3, as is the wetted area as a function of time were sea

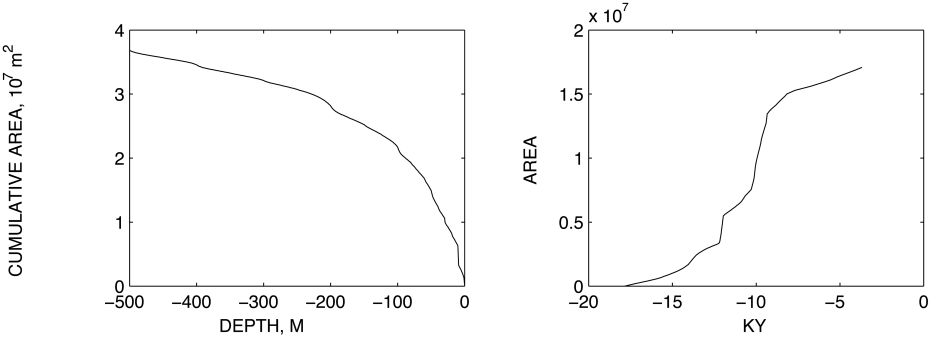

Figure 3. (Left) Cumulative area in m^2 from 0 to 300 m depth (from ETOP05) at 1 meter intervals. (Right) Wetted area shallower than −120 m as a function of time as inferred by linear interpolation from Fairbanks's (1989) curve (^{14}C dates).

level to rise as in Figure 1. Continental shelves do not emerge visually as lying in any particular depth range and, worldwide, appear to exist at a variety of depths above about −100 m. In the event of a uniform rate of rise in sea level, no abrupt change in area is expected—rather a monotonic shift toward increasing the comparatively shallow areas. "Meltwater pulse 1a" (Fig. 2) at about −12,000 y, is what led to the widespread conclusion that injection of freshwater in the North Atlantic generated the following YD and to the rapid increase in area in Figure 3 at that time. The question being raised here is whether such an increase in shallow areas, with corresponding strong tidal dissipation on the shelves and reduction in deep sea tidal mixing, is an alternative mechanism?

Egbert *et al.* (2004) used a modern tidal model to estimate deep water tidal dissipation during the last glacial maximum (LGM) and at rather coarse intervals (5000 years) between then and now. They note that the topography of the LGM is very uncertain, and that in particular, one must account for the significant changes in hypsometry generated by the changing continental ice load. They therefore use the Peltier (1994) reconstruction of global topography during the LGM and the de-glaciation. It is not so easy to determine the accuracy of the topographic reconstruction (see Peltier, 1995). Another major difficulty discussed by Egbert *et al.* (2004) is the sensitivity of the inferred tidal mixing rates to the unknown abyssal stratification of the LGM ocean.

A further major complication is the inference that deep ocean mixing is controlled also by mechanical energy generated by the wind field (Wunsch and Ferrari, 2004). Much of this energy goes into (1) the large-scale circulation and, ultimately, into eddies and, (2) the internal wave field. As the wind field varies through the glacial and interglacial intervals, one would expect a major influence on the abyssal circulation from the varying windstress, both from direct driving of the circulation and through its influence on the abyssal mixing rates—in addition to the effects of tides.

Evidently, full understanding of the implications of abyssal mixing during the de-glaciation will require oceanic GCMs with (1) fully parameterized tidal mixing rates and realistic, (2) topography, (3) stratification, (4) wind-driving, and probably (5) eddy resolution. Achieving this capability is an interesting challenge.

In this present paper, therefore, we restrict ourselves to a purely schematic construction of a vastly oversimplified model. As with a previous paper (Wunsch, 2005), the result is not a description of the oceanic general circulation and its implications, but only the construction of a metaphor that conceivably captures some of the physical elements that would operate, along with many others, in a realistic situation.

4. A simple schematic of a model

We begin by making a schematic model of tidal energy transfer from deep water onto the continental shelf. The model is only to capture some of the basic mechanisms (see, e.g., Egbert *et al.* (2004) for discussion of the elements required for realism). Our tidal model is that of a forced long-wave incident from the open ocean of uniform depth h_2 onto step-like

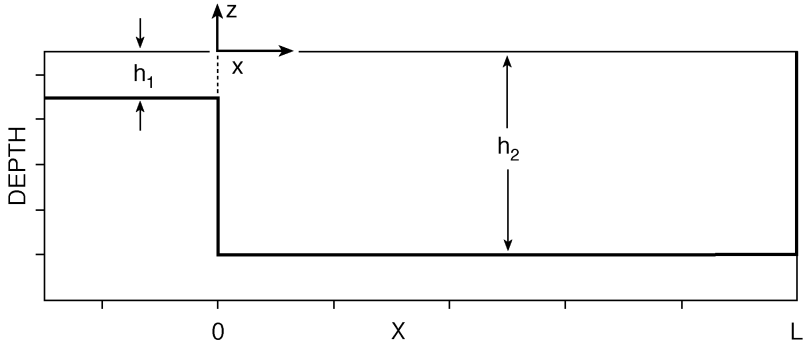

Figure 4. Geometry used to calculate wave dissipation on a shelf. Forced wave is incident from right to left, from deep water to shallow.

continental shelf of depth $h_1 < h_2$ in a nonrotating, otherwise flat-bottom ocean (Fig. 4). The ocean is closed at $x = L$ for the purpose of exploring resonance. The tide disturbing potential is,

$$\bar{\eta}(x, t) = \mathrm{Re}(He^{-(ik_0x + i\sigma t)}), \tag{1}$$

where σ is the (radian) frequency, t is time, x is the coordinate normal to the shelf, that is a forced wave traveling from right to left onto the shelf. $\bar{\eta}$ is assumed to act on both the deep and shallow areas. The governing equations are the linear long-wave equations,

$$\frac{\partial u_j}{\partial t} = -g\frac{\partial(\eta_j - \bar{\eta})}{\partial x} - \varepsilon u_j, \tag{2}$$

$$\frac{\partial \eta_j}{\partial t} + h_j\frac{\partial u_j}{\partial x} = 0 \tag{3}$$

(Lamb, 1932). Here $j = 1, 2$ indicates the variables over the shelf ($j = 1$), and in deep water. ε is a coefficient of bottom friction, producing a linear drag law. It is assumed that ε is the same in both deep and shallow water. Discussion of nonlinear friction is deferred. Nondimensionalization proves convenient: let

$$x = Lx',\ t = \frac{L}{\sqrt{gh_2}}t',\ (u_1, u_2) = H\sqrt{\frac{g}{h_2}}(u_1', u_2'),\ (\eta_1, \eta_2) = H(\eta_1', \eta_2'),\ \varepsilon' = \varepsilon L/\sqrt{gh_2}.$$

The two sets of governing equations become,

$$\frac{\partial u_1}{\partial t} = -\frac{\partial \eta_1}{\partial x} + \frac{\partial \bar{\eta}}{\partial x} - \varepsilon u_1, \tag{4}$$

$$\frac{\partial \eta_1}{\partial t} + \frac{h_1}{h_2}\frac{\partial u_1}{\partial x} = 0, \tag{5}$$

$$\frac{\partial u_2}{\partial t} = -\frac{\partial \eta_2}{\partial x} + \frac{\partial \bar{\eta}}{\partial x} - \varepsilon u_2, \tag{6}$$

$$\frac{\partial \eta_2}{\partial t} + \frac{\partial u_2}{\partial x} = 0, \tag{7}$$

and where the primes on the variables have been dropped. The nondimensional equilibrium tide is then,

$$\bar{\eta} = \exp(-(ik_0' x + i\sigma' t)), \quad k_0' = k_0 L, \quad \sigma' = \frac{L}{\sqrt{gh_2}}\sigma,$$

and these primes will now also be dropped.

A particular solution in each region is

$$u_j(x, t) = \frac{k_0 \sigma}{\sigma\tilde{\sigma} - k_0^2}\exp(-(ik_0 x + i\sigma t)), \tag{8}$$

$$\begin{aligned} \tilde{\sigma} &= \sigma + i\varepsilon \\ \eta_j(x, t) &= -\frac{h_j}{h_2}\frac{k_0}{\sigma}u_j, \quad j = 1, 2. \end{aligned} \tag{9}$$

There are two homogeneous solutions (positive and negative traveling) in each of the two regions, leaving four unknown coefficients to be determined by boundary/matching/radiation conditions. At $x = L$, the boundary condition is $u_2 = 0$. The (dimensional) matching conditions at $x = 0$ are,

$$\eta_1|_{x=0} = \eta_2|_{x=0}, \tag{10}$$

$$h_1 u_1|_{x=0} = h_2 u_2|_{x=0}, \tag{11}$$

that is, continuity of pressure and mass flux, respectively. In region 1, the radiation condition precludes a wave traveling in the $+x$ direction. Use of the hydrostatic equations in a patently nonhydrostatic region (next to the step), as done by Lamb (1932) and his successors, is obviously invalid. Bartholomeusz (1958) shows, however, after an elaborate calculation, that one nonetheless obtains the correct transmission and reflection coefficients. Miles (1967) discusses the problem more generally.

The ratio h_1/h_2 controls how much energy is transmitted from the deep ocean to the shelf. In the present configuration, all energy on the shelf is removed from the system. In deep water, there is a competition between the possibility of resonance (as $h_1 \to 0$, so that the deep basin becomes entirely enclosed), and the tendency of energy to be lost through

transmission into shallow water. In the limit $h_1 = 0$, one can have a true resonance (apart from the frictional damping which keeps the motion bounded), and a large deep water tidal dissipation.

A dimensional energy equation is,

$$\frac{\partial(u_j^2 h_i/2 + g\eta_j^2/2)}{\partial t} = -gh_j \frac{\partial(u_j(\eta_j - \bar{\eta}))}{\partial x} - \varepsilon u_j^2 h_j. \tag{12}$$

It is assumed here that all of the energy moving onto the shelf in one wave cycle,

$$F = g\overline{u_2\eta_2}h_2, \tag{13}$$

is dissipated there (ignoring the flux of equilibrium tide energy). An overbar indicates a time average over one period. The energy dissipated in the deep basin is

$$D_2 = \varepsilon h_2 \int_0^L \overline{u_2(x)^2} dx,$$

and will be identified with that available to mix the abyss. Note that in the real system, deep water energy loss is believed to occur primarily through scattering rather than through friction (e.g., Jayne and St. Laurent, 2001; Egbert *et al.,* 2004).

If $\varepsilon = 0$, and with $h_1 = 0$, the deep basin will resonate whenever $\sigma = n\pi$, with n an integer. (A traveling wave resonance can exist when the denominator of Eq. (8) vanishes, and $h_1 = h_2$, but for simplicity we will avoid that situation.) Figure 5 shows the flux into shallow water as a function of h_1/h_2 for three sets of frequencies, including one near-resonance. At low frequencies, far from resonance, the flux decreases monotonically to zero in the limit as $h_1/h_2 \to 0$. In contrast, near resonance, the flux reaches a maximum as the shelf depth becomes small, and a closed resonant system is approached, but then decreases again as the shelf water depth becomes too small to permit significant transmission. At frequencies above resonance, dissipation also reaches a maximum with h_1/h_2 before diminishing again as the basin becomes closed. A zero in transmission occurs at high frequencies, above resonance, dependent upon σ.

Dissipation within the deep basin also behaves differently near and far from resonance (Fig. 6). Below resonance, there is a general monotonic dissipation decrease as $h_1/h_2 \to 0$, while at resonance and at frequencies above, dissipation increases abruptly in this limit. Evidently a discussion of how rapidly deep water dissipation will diminish (or increase) as shelves become water-covered will depend upon the proximity of tidal resonances in the particular basin. Note that the modern North Atlantic appears to have a resonance at about 13 hours (e.g., Platzman, 1991) and it is conceivable that in a slightly smaller basin with lower sea level, that the glacial North Atlantic would have been close to resonance at the lunar semi-diurnal period of 12.42 hours. Other near-resonances of the global ocean are known (e.g., Platzman, 1991; Egbert *et al.,* 2004).

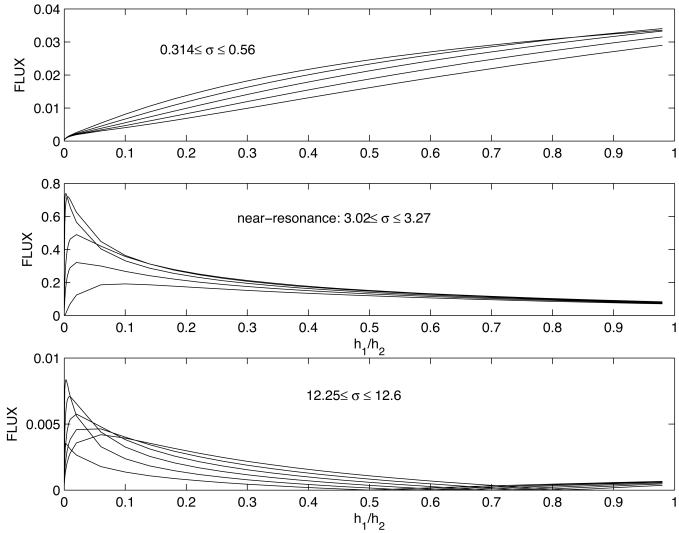

Figure 5. Flux into shallow water as a function of h_1/h_2. Three sets of curves are shown—one at low frequency (upper), one centered on the lowest near-resonance at $\sigma' = \pi$ (middle), and one at frequencies above resonance. Note changing scales.

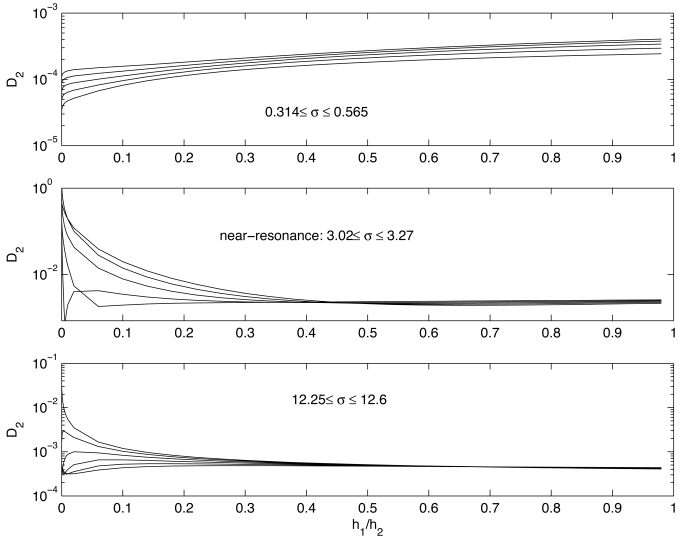

Figure 6. Same as Figure 5 except representing the net dissipation in the deep basin. $\varepsilon = 0.1$. Note changing scales.

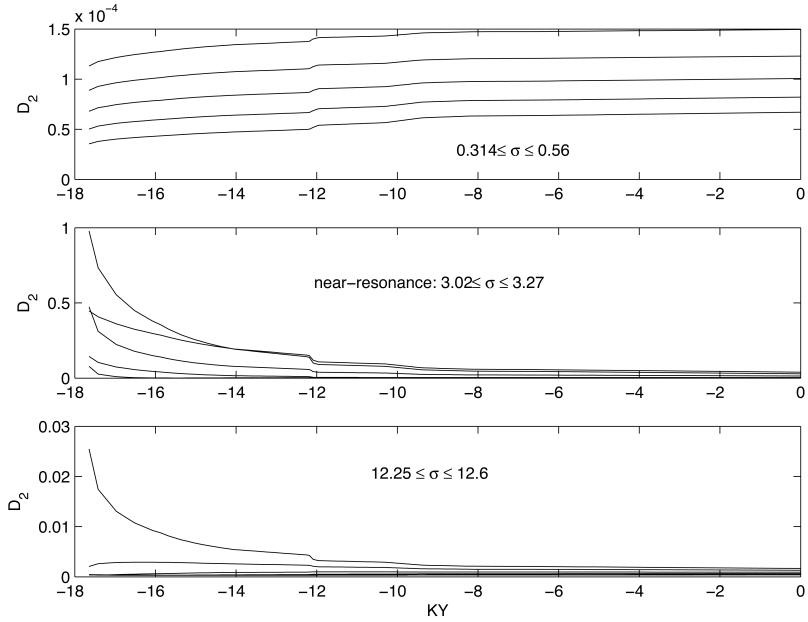

Figure 7. Net dissipation in deep water as a function of time (radiocarbon years) for the same frequencies in Figure 5. It is assumed that at $t = -17.8$ ky that $h_1 = 0$, and that it increases to 120 m at $t = 0$, following the Bard *et al.* curve. Away from resonance (upper) dissipation increases slightly with time. Middle panel displays near-resonant frequencies, and lower panel frequencies above resonance. ($\varepsilon = 0.1$). Note changing scales.

Figure 7 displays the deep water dissipation, D_2, as a function of time, taking the Bard *et al.* (1990) depth change as being correct. A minor near-discontinuity occurs at about the time of the YD, but otherwise a smooth variation is inferred. These results, despite the enormous simplifications relative to a realistic tidal model, suggest some simple experiments concerning the implications for the circulation of a time-changing mixing rate.

5. Wind effects

As stated in the Introduction, present thinking suggests roughly equal control of oceanic mixing energetics by tides and winds. Oceanic kinetic energies (a measure of flow rates) are dominated by the mesoscale (Wunsch and Ferrari, 2004; note that in their Fig. 5—the summary of ocean energetics—the value for the internal wave energy should be 1.4 Exajoules, rather than the 14 Exajoules shown. Mesoscale energy is a factor of 10 larger than that for internal waves (S. Thorpe, pers. comm., 2004). As Wunsch and Ferrari (2004) point out, little is known about where the mesoscale energy is dissipated. Much like the tides, however, one anticipates that interaction with topography is a potential major

contributor. To the extent that mesoscale eddy energy is, like the tides, dissipated in the coastal regions, changes in boundary topography with changing sea level could have a major effect on the mesoscale-induced mixing. (Of course, changes in the strength of the wind field can also have a major influence on the intensity of mesoscale eddies through the instabilities of the large-scale general circulation. Any complete understanding of time-varying ocean mixing must account for a modified wind field, but in the absence of any quantitative estimates of winds through time, we set aside this potentially dominant factor.)

A considerable literature, both theoretical and observational, exists on the low frequency variability in coastal regions (e.g., LeBlond and Mysak, 1978; Miller, 1986; Chapman and Brink, 1987; Huthnance, 1995; Greatbatch *et al.,* 1996; Brink, 1998; etc.), but there seems to be no existing estimate of the global rate of mesoscale energy dissipation there. Because $\sigma \ll f$, where f is the local Coriolis parameter, one anticipates that the continental slope/rise, rather than the shelf region, would predominantly affect the mesoscale. That is, excitation of topographically trapped waves by incoming eddies is to be expected. Brink (1998), in particular, notes that little mesoscale-frequency band energy is observed on the shelf itself.

In the absence of understanding of the coupling between slope and deep water in the mesoscale band, and the gross uncertainty of the topographic slopes during the deglaciation, it would be a brave individual who would attempt now to estimate mixing variations by oceanic mesoscale eddies owing to changing global water depths. We leave it as an important piece of business to be dealt with in the future.

6. The loop-Stommel model

Can one gain some insight into how a reduction in available mixing in the abyss could affect the ocean circulation? Stommel's (1961) two box model (Fig. 8) has often been invoked as explaining multiple ocean states. A very large literature has grown, identifying the two-states of this model with both GCM behavior and inferred past climate (for example, Clark *et al.,* 2002). In a separate paper (Wunsch, 2004; hereafter W2004), one can find a discussion of its equivalence to a one-dimensional loop model, but with the additional features of permitting explicit control of the mixing rates, which are fixed at infinity and zero in Stommel's original. He found two stable states, a "salinity mode," with $w' > 0$, carrying upper-level fluid from cold to warm, and a stronger "thermal mode" with $w' < 0$, warm to cold flow. Any plausible discussion of the ocean circulation must include the wind stress, and the model was extended in W2004 to include such a stress; it significantly complicates the discussion.

Diffusion is parameterized here by an *inverse* Rayleigh number, $R = Ra^{-1}$, which is proportional to the diffusion coefficient. The notion is to understand the extent to which the system changes state when R is allowed to be a function of t, in either a step change or through a continuous decrease, as suggested by Figure 7. In a system with changing

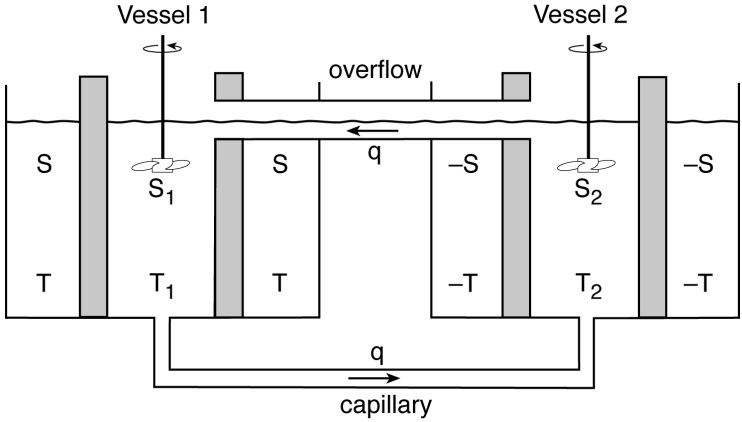

Figure 8. Redrawn version of box model used by Stommel (1961) to mimic the response of the ocean to forced temperature and salinity boundary conditions. Each box is supposed well-mixed with the temperature and salinity values relaxed toward the surrounding imposed temperatures and salinities ($\pm S$, $\pm T$). Flow between the boxes takes place in the connecting capillary tubes. The model is isomorphic to a one-dimensional fluid loop.

diffusion, one might argue that the Prandtl number, Pr, should also change. Here, however, we have opted to fix Pr.

This loop model (see Fig. 9) is described by the momentum equation in the ϕ coordinate, and corresponding heat and salt equations in one dimension. Here (salt) and cold (fresh) sources are placed at $\phi = \phi_+ = -\phi_-$ to resemble the heating/cooling, freshening/salinification at the same depth (geopotential) as in the real ocean. In addition, a temperature restoring $\gamma(T^*(\phi) - T(\phi, t))$ is used to mimic the surface boundary conditions often used in GCMs. T^* is an externally imposed temperature, here proportional to sin ϕ. A large literature exists on buoyancy-driven loop flows in both engineering and science applications, including Tritton (1988) and Dewar and Huang (1996). See W2004 for a fuller discussion and additional references.

In addition to R and Pr, nondimensional parameters of the problem include the *inverse* salt Rayleigh number, R_S, a nondimensional temperature restoring coefficient, γ', and a stress, τ'. Here the primes will be retained; they denote nondimensional variables pertaining to the loop, not the tidal model. Transient behavior of this simple loop is remarkably complex, involving the many nondimensional parameters, as well as the initial conditions and time histories of the heat and salt sources. No attempt is made here to explore the full range of possibilities. We do, however, focus on parameter ranges in which shifts in mixing rates are capable of producing "interesting" results. The nondimensional flow field is $w'(t')$, where t' is the corresponding dimensionless time (measured in units of $\sqrt{aR/g\Delta_T H}$; Δ_T is the coefficient of thermal expansion, and H is the heat source strength).

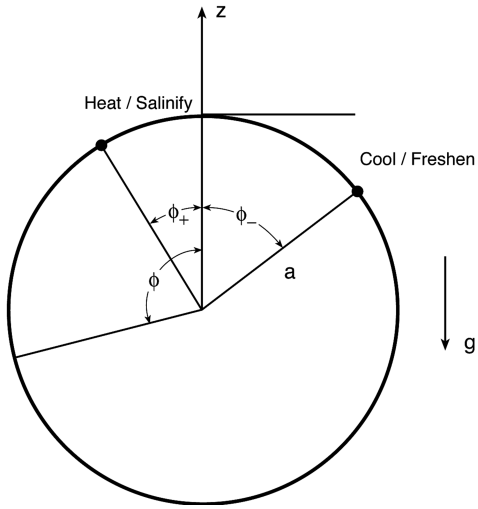

Figure 9. Geometry of loop-Stommel model. Radius is a, azimuthal angle, ϕ. Heat/salt sources/sinks are at $\phi = \phi_\pm$. Here $\phi_+ = -\phi_-$ so that heating and cooling take place at the same level, mimicking the ocean situation. The one-dimensional flow is w' in nondimensional units. See W2004 for details.

Figures 10 and 11 show the time history of $w'(t')$, the azimuthal velocity, for a particular choice of parameters ($R = R_S = 1$, $Pr = 1$, $\gamma' = 1$, $\tau' = \pm 1$). Initial conditions are, $T'(\phi, 0) = S'(\phi, 0) = 0$, but two different initial conditions for w' are used, $w'(0) = 0$, and $w'(0) = \tau'$, because in some cases discussed by W2004, different asymptotes result (but not in this particular parameter range). At $t' = 50$, $R = R_S$ are reduced to 0.1, toward the larger end of the possibilities suggested by the tidal model. That is, the heat and salt diffusion are reduced to 10% of their previous values, attempting to mimic the reduction in deep water tidal dissipation energy seen when continental shelves are covered by rising sea level. Evidently a change in diffusion can qualitatively and quantitatively change the flow (and hence the heat transport) patterns. Particularly striking is the oscillatory behavior seen in Figure 11.

Figure 12 shows the loop displayed as an analogue to the S61 box model, with the loop opened out into two basins of arbitrary "latitude" range, as in W2004. Two steady states corresponding to the different values of R, w' are shown. The corresponding heat flux at $\phi = 0$ is shown in Figure 13, along with the temperature distribution in the loop just prior to the adjustment in R, R_S, and at the final time. With the eye of faith, one might connect such oscillations in heat flux to those seen in the foraminiferal $\delta^{18}O$ data shown by McManus *et al.* (2004, their Fig. 1). Such shifts in oceanic meridional heat flux, associated with the mass flux changes would have many climate impacts, but there are limits beyond which speculation should not be carried.

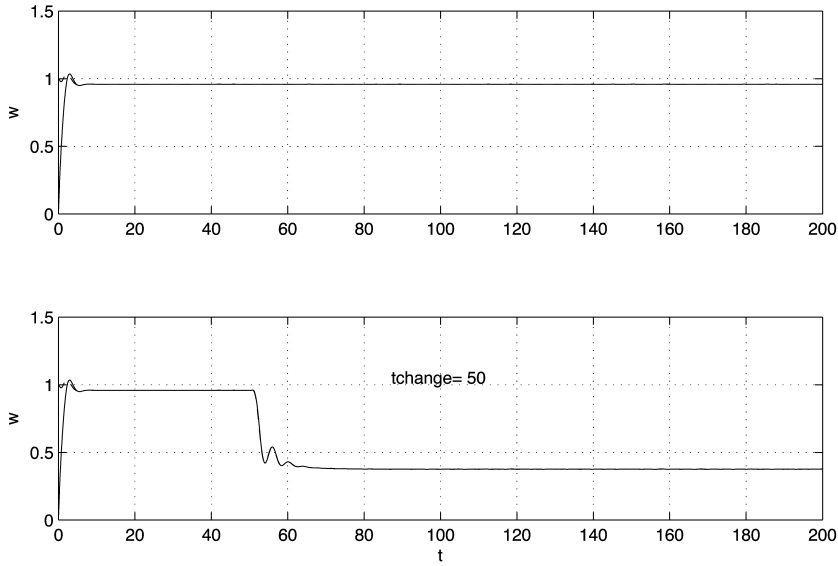

Figure 10. (Upper panel). Time history, $w'(t')$ starting with $R = 1$, $\tau' = 1$, with initial conditions $w'(0) = 0$ (solid curve) and $w'(0) = \tau'$ (dashed). In this parameter range, the different starting conditions do not affect the asymptotic state, and they are treated as a single solution. (Lower panel) At $t' = 50$, R is decreased by 90% resulting in a different asymptote. Here, the two starting conditions make no difference in the asymptotic value. $w' > 0$ corresponds to the S61 salinity mode, and $w' < 0$ to the thermal mode.

Given the results so far, one anticipates that the history of the change in R, R_S will have an influence on the flow and heat flux itself. Figure 3, if taken literally, suggests that the diffusion coefficient more likely shifted gradually, rather than abruptly. As one example of the effects of such a change, Figure 14 shows the same parameter range as in Figures 11 and 13 except that R, R_S were lowered slowly (linearly) between $t' = 50$ and $t' = 150$. Note that oscillatory behavior does not set in until well after the final diffusion coefficient values have been set. As noted earlier, the complex behavior of the model does not seem to depend upon details of the de-glaciation and sea level rise.

7. Comments

As discussed in W2004, by appropriate choice of parameters, in a one-dimensional system with buoyancy forcing fixed to one level, one can obtain a very wide range of interesting temporal and steady behaviors (the governing equations are, apart from some source terms, those of Lorenz). The equation remains, however, as to whether any of these results for a one-dimensional fluid loop have application to the real climate system? A fluid

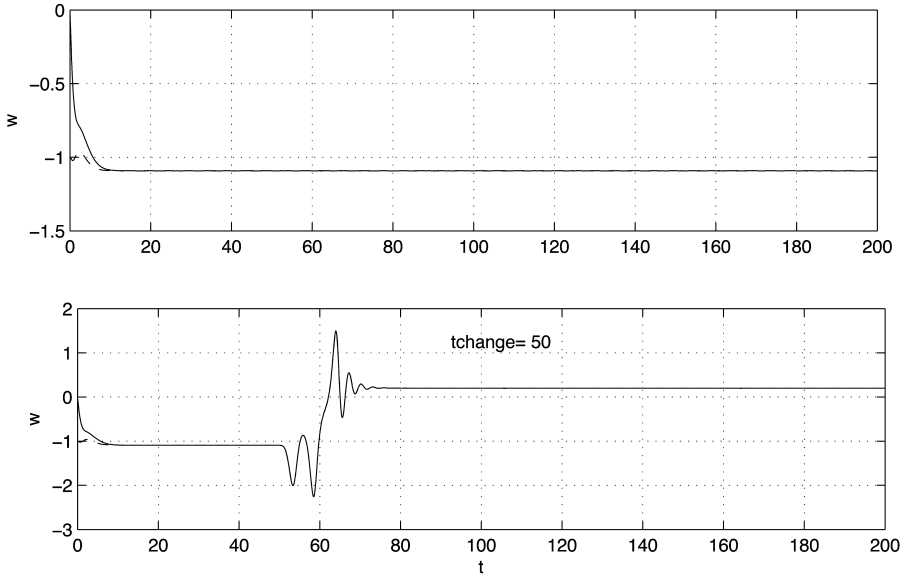

Figure 11. Same as Figure 10 except that now $\tau' = -1$. Note oscillatory behavior after the change in R and the reversal in the sign of the asymptotic w'. Whether apparent oscillations in the deglaciating climate state are related to this phenomenon is unknown. Again, different initial conditions on w' produce solution differences only very near $t' = 0$. Overall, the shift is from the thermal to the salinity mode with wind stress playing an important role.

loop, and the Stommel (1961) box model to which it is isomorphic, are essentially described by three degrees of freedom. Very little is known about the relationship of such low-dimensional models and the extremely high dimension of the coupled atmosphere and ocean (and ice). The connection between Rayleigh or Prandtl numbers characteristic of the ocean as a whole, and the single values assigned in a fluid loop is very obscure.

W2004 used the loop-Stommel models as a metaphor for the ocean circulation. They have a role in suggesting conceivable behavior of the far more complex real or GCM oceans. In the absence, however, of a method for representing high dimensional systems in terms of low dimensional ones, particularly where there is concern over systematic model errors integrated over long climate time scales, one is driven to employ the full models as far as practicable. At best, the low-dimensional result suggests behavior one might look for in a more complete system. Should one desire, even the loop models can be made considerably more complex. Easy extensions would include double-diffusive motions produced by using differing heat and salt inverse Rayleigh numbers (e.g., Schmitt, 1994), and instabilities from nonlinearities in the equation of state (e.g., Fofonoff, 2001). The impact of the use of a salinity boundary condition, rather than the more appropriate one for freshwater (Huang, 1993), should also be explored.

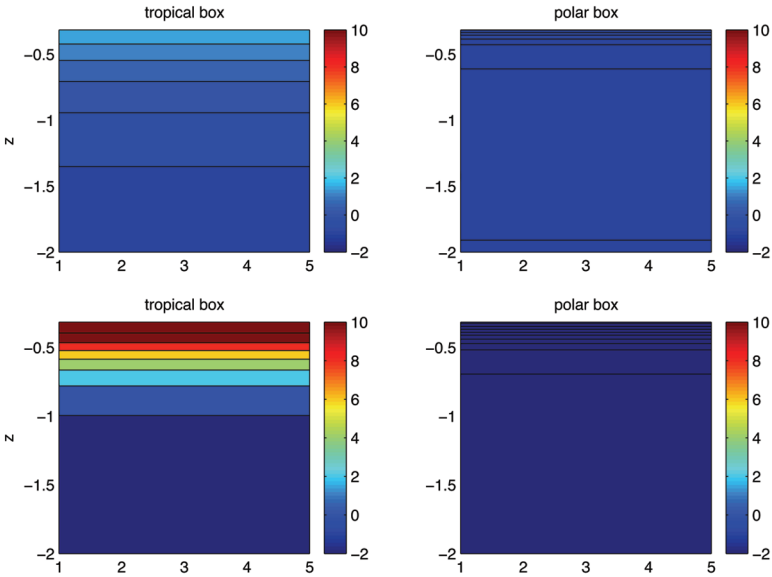

Figure 12. The thermal loop temperature field displayed in the analogue to the S61 form, as though the loop is spread into two basins. The "tropical" box is the region below the heat/salt source to $\phi = \pi$, and the "polar" box lies below the cold/fresh source to $\phi = -\pi$. Widths of the boxes are arbitrary. The situation is the same as in Figure 11. Top two boxes are the asymptotic steady state temperatures at time $t' = 40$, with $w = -1.09$, $R = 1$, and the bottom two correspond to $t' = 200$, with $w' = +0.20$, $R = 0.1$. The temperature restoring coefficient is $\gamma' = 1$. The tropical box stratification is the most sensitive in this parameter range.

Extending the present schematic to the real ocean involves several serious steps: (1) A full tidal model is required. The detailed dynamics of modern ocean tides involve specification of the correct topography, rotation, the spherical harmonic description of the equilibrium tide, and a prescription of the dissipation mechanisms (e.g., Egbert *et al.,* 2004). Whether a truly baroclinic model is required to properly represent the scattering into

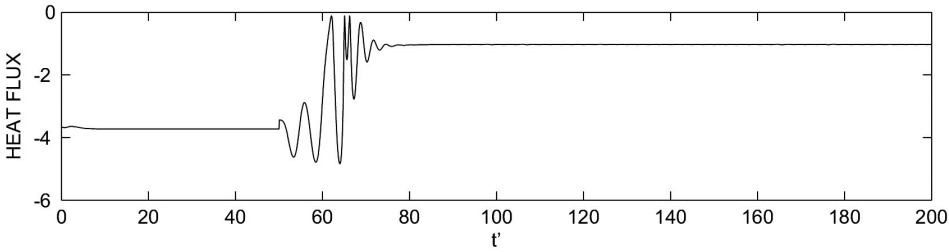

Figure 13. Nondimensional heat flux at the top center of the loop as a function of time. Fluctuations in w' and R produce a changing heat flux toward the cold source.

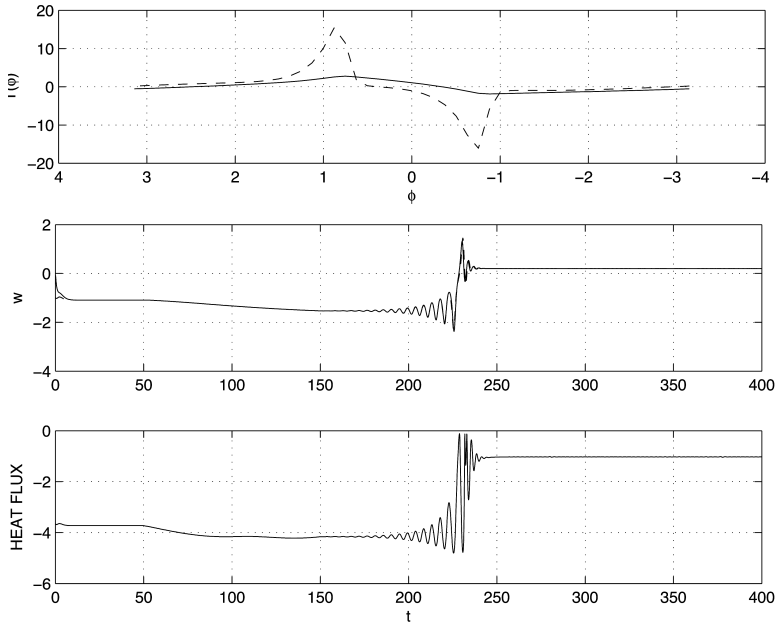

Figure 14. (Middle) $w'(t')$ corresponding to 11, except that R, R_S are lowered linearly in time $50 \leq t' \leq 150$. (Top) Temperature just prior to $t' = 50$ (solid) and again at $t' = 400$ (dashed). (Bottom) Nondimensional heat flux at $\phi = 0$, as a function of time.

internal tides is still unclear. (2) An oceanic general circulation model (GCM) with realistic depiction of oceanic mixing. Such a GCM does not now exist. Some indication of its importance, however, can be inferred from a recent paper of Simmons *et al.* (2004). They compared the heat flux in a GCM with a conventional horizontally uniform mixing coefficient to one in which the mixing was parameterized so as to partially represent the effects of spatially nonuniform, and abyssally enhanced tidal mixing. A major change in the poleward heat flux of the model was found. (3) Ultimately, any such calculation has to be done with a coupled ocean/atmosphere/cryosphere model: sizeable shifts in the ocean circulation would bring about large changes in atmospheric winds, buoyancy exchange, and oceanic sea ice cover. The tidal element of this story can, all by itself, be rendered much more interesting and complete. With real geometry, changing proximity to deep-water resonances, rotation, coastal reflections, and nonlinear friction, a rise in sea level can lead to either an increase or decrease in the dissipation on the shelf. Oceanic mesoscale dissipation on the continental slope regions—with its sensitivity to topographic gradients and variations in wind stress—is also likely to be important, but is not considered here.

No claim is made that the Younger Dryas has been explained. We have merely suggested the possibility that abyssal mixing shifts connected with the de-glaciation could upset the oceanic meridional heat flux and consequently the sea-surface temperature.

Whether such an explanation can survive tests with realistic high resolution, coupled, models remains to be seen. It is possible that none of the mechanisms suggested for causing the YD will survive the shift to realistic models, or that all of them, acting in concert, are required.

Acknowledgments. Helpful comments were provided by M. Munk, P. Huybers, O. Marchal, and S. Yuan. D. Mohrig made the hypsometric curve data available in convenient form.

REFERENCES

Bard, E., B. Hamelin and R. G. Fairbanks. 1990. U-Th ages obtained by mass-spectrometry in corals from Barbados—sea-level during the past 130,000 years. Nature, *346,* 456–458.

Bartholomeusz, E. F. 1958. The reflection of long waves at a step. Proc. Camb. Phil. Soc., *54,* 106–118.

Bradley, R. S. 1999. Paleoclimatology, 2nd ed., Academic, San Diego, 610 pp.

Brink, K. 1998. Deep-sea forcing and exchange processes, *in* The Sea, *10,* K. H. Brink and A. R. Robinson, eds., 151–167.

Chapman, D. C. and K. H. Brink. 1987. Shelf and slope circulation induced by fluctuating offshore forcing. J. Geophys. Res., *92,* 11,741–11,759.

Clark, P. U., N. G. Pisias, T. F. Stocker and A. J. Weaver. 2002. The role of the thermohaline circulation in abrupt climate change. Nature, *415,* 863–869.

Dewar, W. K. and R. X. Huang. 1996. On the forced flow of salty water in a loop. Phys. Fluids, *8,* 954–970.

Egbert, G. D., R. D. Ray and B. G. Bills. 2004. Numerical modeling of the global semidiurnal tide in the present day and in the last glacial maximum. J. Geophys. Res., *109(C3),* C03003, doi: 10.1029/2003JC001973.

Fairbanks, R. G. 1989. A 17,000 year glacio-eustatic sea level record: influence of glacial melting rates on the Younger Dryas event and deep ocean circulation. Nature, *342,* 637–642.

Fofonoff, N. P. 2001. Thermal stability of the world ocean thermoclines. J. Phys. Oceanogr., *31,* 2169–2177.

Gill, A. E. 1982. Atmosphere-Ocean Dynamics, Academic Press, NY, 662 pp.

Greatbatch, R. J., Y. Lu and B. deYoung. 1996. Application of a barotropic model to North Atlantic synoptic sea level variability. J. Mar. Res., *54,* 451–469.

Huang, R.-X. 1993. Real fresh-water flux as a natural boundary-condition for the salinity balance and thermohaline circulation forced by evaporation and precipitation. J. Phys. Oceanogr., *23,* 2428–2446.

Huthnance, J. M. 1995. Circulation, exchange and water masses at the ocean margin: the role of physical processes at the shelf edge. Prog. Oceanogr., *35,* 353–431.

Jayne, S. R. and L. C. St. Laurent. 2001. Parameterizing tidal dissipation over rough topography. Geophys. Res. Lett., *28,* 811–814.

Lamb, H. 1932. Hydrodynamics, 6th ed., Dover, NY, 738 pp.

LeBlond, P. H. and L. Mysak. 1978. Waves in the Ocean, Elsevier, Amsterdam, 602 pp.

Lehman, S. J. and L. D. Keigwin. 1992. Sudden changes in North Atlantic circulation during the last glaciation. Nature, *356,* 757–762.

McManus, J. F., R. François, J.-M. Gherardi, L. D. Keigwin and S. Brown-Leger. 2004. Collapse and rapid resumption of Atlantic meridional overturning circulation linked to deglacial climate changes. Nature, *428,* 834–837.

Miles, J. W. 1967. Surface-wave sccattering matrix for a shelf. J. Fluid Mech., *28,* 755–767.

Miller, A. J. 1986. Nondivergent planetary oscillations in midlatitude ocean basins with continental shelves. J. Phys. Oceanogr., *16,* 1914–1928.

Munk, W. and C. Wunsch. 1998. Abyssal recipes II: energetics of tidal and wind mixing. Deep-Sea Res., *45,* 1976–2009.

Nilsson, J., G. Broström and G. Walin. 2003. The thermohaline circulation and vertical mixing: does weaker density stratification give stronger overturning? J. Phys. Oceanogr., *33,* 2781–2795.

Peltier, W. R. 1994. Paleotopography of glacial-age ice sheets. Science, *265,* 195–201.

—— 1995. Paleotopography of glacial-age ice sheets—Reply. Science, *267,* 536–538.

Platzman, G. W. 1991. Tidal evidence for ocean normal modes, *in* Tidal Hydrodynamics, B. B. Parker, ed., John Wiley, NY, 13–26.

Saltzman, B. 2002. Dynamical Paleoclimatology. Generalized Theory of Global Climate Change. Academic, San Diego, 354 pp.

Schmitt, R. W. 1994. Double diffusion in oceanography. Ann. Rev. Fluid Mech., *26,* 255–285.

Simmons, H. L., S. R. Jayne, L. C. St. Laurent and A. J. Weaver. 2004. Tidally driven mixing in a numerical model of the ocean circulation. Ocean Model., *3–4,* 245–263.

Stommel, H. 1961. Thermohaline convection with two stable regimes of flow. Tellus, *13,* 131–149.

Tritton, D. J. 1988. Physical Fluid Dynamics, 2nd ed., Oxford Univ. Press, Oxford, 519 pp.

Wunsch, C. 2005. Thermohaline loops, Stommel box models and Sandström's theorem. Tellus, *57A,* 84–99.

Wunsch, C. and R. Ferrari. 2004. Vertical mixing, energy, and the general circulation of the oceans. Ann. Rev. Fluid Mech., *36,* doi:10.1146/annurev.fluid.36.050802.122121.

Received: *28 June, 2004;* revised: *25 October, 2004.*